# Early time solution as an alternative to the late time evolving dark energy with DESI DR2 BAO

```
E. Chaussidon<sup>0</sup>, <sup>1,*</sup> M. White<sup>0</sup>, <sup>2,3</sup> A. de Mattia<sup>0</sup>, <sup>4</sup> R. Gsponer<sup>0</sup>, <sup>5</sup> S. Ahlen<sup>0</sup>, <sup>6</sup> D. Bianchi<sup>0</sup>, <sup>7,8</sup> D. Brooks, <sup>9</sup> T. Claybaugh, <sup>1</sup> S. Cole<sup>0</sup>, <sup>10</sup> A. Cuceu<sup>0</sup>, <sup>1</sup> A. de la Macorra<sup>0</sup>, <sup>11</sup> P. Doel, <sup>9</sup> S. Ferraro<sup>0</sup>, <sup>1,3</sup> A. Font-Ribera<sup>0</sup>, <sup>12</sup> J. E. Forero-Romero<sup>0</sup>, <sup>13,14</sup> E. Gaztañaga, <sup>15,16,17</sup> S. Gontcho A. Gontcho, <sup>1</sup> G. Gutierrez, <sup>18</sup> J. Guy<sup>0</sup>, <sup>1</sup> C. Hahn<sup>0</sup>, <sup>19</sup> H. K. Herrera-Alcantar<sup>0</sup>, <sup>20,4</sup> K. Honscheid<sup>0</sup>, <sup>21,22,23</sup> M. Ishak<sup>0</sup>, <sup>24</sup> D. Kirkby<sup>0</sup>, <sup>25</sup> T. Kisner<sup>0</sup>, <sup>1</sup> A. Kremin<sup>0</sup>, <sup>1</sup> M. Landriau<sup>0</sup>, <sup>1</sup> L. Le Guillou<sup>0</sup>, <sup>26</sup> M. E. Levi<sup>0</sup>, <sup>1</sup> R. Miquel, <sup>27,12</sup> J. Moustakas<sup>0</sup>, <sup>28</sup> G. Niz<sup>0</sup>, <sup>29,30</sup> W. J. Percival<sup>0</sup>, <sup>31,32,33</sup> F. Prada<sup>0</sup>, <sup>34</sup> I. Pérez-Ràfols<sup>0</sup>, <sup>35</sup> A. J. Ross<sup>0</sup>, <sup>21,36,23</sup> G. Rossi, <sup>37</sup> E. Sanchez<sup>0</sup>, <sup>38</sup> D. Schlegel, <sup>1</sup> H. Seo<sup>0</sup>, <sup>39</sup> D. Sprayberry, <sup>40</sup> M. Walther<sup>0</sup>, <sup>41,42</sup> and B. A. Weaver<sup>40</sup>
                          <sup>1</sup>Lawrence Berkeley National Laboratory, 1 Cyclotron Road, Berkeley, California 94720, USA
                              <sup>2</sup>Department of Physics, University of California, Berkeley, 366 LeConte Hall MC 7300,
                                                                   Berkeley, California 94720-7300, USA
                        <sup>3</sup>University of California, Berkeley, 110 Sproul Hall No. 5800 Berkeley, California 94720, USA
                                            <sup>4</sup>IRFU, CEA, Université Paris-Saclay, F-91191 Gif-sur-Yvette, France
                    <sup>5</sup>Institute of Physics, Laboratory of Astrophysics, École Polytechnique Fédérale de Lausanne (EPFL),
                                      Observatoire de Sauverny, Chemin Pegasi 51, CH-1290 Versoix, Switzerland
                    <sup>6</sup>Physics Department, Boston University, 590 Commonwealth Avenue, Boston, Massachusetts 02215, USA
                                      <sup>7</sup>Dipartimento di Fisica "Aldo Pontremoli," Università degli Studi di Milano,
                                                                    Via Celoria 16, I-20133 Milano, Italy
                                      <sup>8</sup>INAF-Osservatorio Astronomico di Brera, Via Brera 28, 20122 Milano, Italy
                                             <sup>9</sup>Department of Physics and Astronomy, University College London,
                                                         Gower Street, London, WC1E 6BT, United Kingdom
                                <sup>10</sup>Institute for Computational Cosmology, Department of Physics, Durham University,
                                                           South Road, Durham DH1 3LE, United Kingdom
                    <sup>11</sup>Instituto de Física, Universidad Nacional Autónoma de México, Circuito de la Investigación Científica,
                                                   Ciudad Universitaria, Ciudad de México CP 04510, México
                        <sup>12</sup>Institut de Física d'Altes Energies (IFAE), The Barcelona Institute of Science and Technology,
                                                Edifici Cn, Campus UAB, 08193, Bellaterra (Barcelona), Spain
                                <sup>13</sup>Departamento de Física, Universidad de los Andes, Cra. 1 No. 18A-10, Edificio Ip,
                                                                        CP 111711, Bogotá, Colombia
                                        <sup>14</sup>Observatorio Astronómico, Universidad de los Andes, Cra. 1 No. 18A-10,
                                                                Edificio H, CP 111711 Bogotá, Colombia
                               <sup>15</sup>Institut d'Estudis Espacials de Catalunya (IEEC), c/ Esteve Terradas 1, Edifici RDIT,
                                                             Campus PMT-UPC, 08860 Castelldefels, Spain
                           <sup>16</sup>Institute of Cosmology and Gravitation, University of Portsmouth, Dennis Sciama Building,
                                                                  Portsmouth, PO1 3FX, United Kingdom
                                 <sup>17</sup>Institute of Space Sciences, ICE-CSIC, Campus UAB, Carrer de Can Magrans s/n,
                                                                     08913 Bellaterra, Barcelona, Spain
                                <sup>18</sup>Fermi National Accelerator Laboratory, P.O. Box 500, Batavia, Illinois 60510, USA
                      <sup>19</sup>Steward Observatory, University of Arizona, 933 N. Cherry Avenue, Tucson, Arizona 85721, USA
                                    <sup>20</sup>Institut d'Astrophysique de Paris. 98 bis boulevard Arago 75014 Paris, France
                    <sup>21</sup>Center for Cosmology and AstroParticle Physics, The Ohio State University, 191 West Woodruff Avenue,
                                                                          Columbus, Ohio 43210, USA
                                    <sup>22</sup>Department of Physics, The Ohio State University, 191 West Woodruff Avenue,
                                                                          Columbus, Ohio 43210, USA
                                                    <sup>23</sup>The Ohio State University, Columbus, 43210 Ohio, USA
                               <sup>24</sup>Department of Physics, The University of Texas at Dallas, 800 West Campbell Road,
                                                                        Richardson, Texas 75080, USA
                        <sup>25</sup>Department of Physics and Astronomy, University of California, Irvine, California 92697, USA
                    <sup>26</sup>Sorbonne Université, CNRS/IN2P3, Laboratoire de Physique Nucléaire et de Hautes Energies (LPNHE),
                                                                             FR-75005 Paris, France
                                   <sup>27</sup>Institució Catalana de Recerca i Estudis Avançats, Passeig de Lluís Companys,
                                                                           23, 08010 Barcelona, Spain
                                        <sup>28</sup>Department of Physics and Astronomy, Siena College, 515 Loudon Road,
```

Loudonville, New York 12211, USA

```
<sup>29</sup>Departamento de Física, DCI-Campus León, Universidad de Guanajuato,
                    Loma del Bosque 103, León, Guanajuato C. P. 37150, México
   <sup>30</sup>Instituto Avanzado de Cosmología A. C., San Marcos 11—Atenas 202, Magdalena Contreras,
                                Ciudad de México C. P. 10720, México
     <sup>31</sup>Department of Physics and Astronomy, University of Waterloo, 200 University Avenue W,
                                  Waterloo, Ontario N2L 3G1, Canada
                <sup>32</sup>Perimeter Institute for Theoretical Physics, 31 Caroline Street North,
                                  Waterloo, Ontario N2L 2Y5, Canada
        <sup>33</sup>Waterloo Centre for Astrophysics, University of Waterloo, 200 University Avenue W,
                                  Waterloo, Ontario N2L 3G1, Canada
<sup>34</sup>Instituto de Astrofísica de Andalucía (CSIC), Glorieta de la Astronomía, s/n, E-18008 Granada, Spain
    <sup>35</sup>Departament de Física, EEBE, Universitat Politècnica de Catalunya, c/Eduard Maristany 10,
                                        08930 Barcelona, Spain
        <sup>36</sup>Department of Astronomy, The Ohio State University, 4055 McPherson Laboratory,
                          140 West 18th Avenue, Columbus, Ohio 43210, USA
           <sup>37</sup>Department of Physics and Astronomy, Sejong University, 209 Neungdong-ro,
                             Gwangjin-gu, Seoul 05006, Republic of Korea
                     <sup>38</sup>CIEMAT, Avenida Complutense 40, E-28040 Madrid, Spain
          <sup>39</sup>Department of Physics and Astronomy, Ohio University, 139 University Terrace,
                                       Athens, Ohio 45701, USA
              <sup>40</sup>NSF NOIRLab, 950 North Cherry Avenue, Tucson, Arizona 85719, USA
          <sup>41</sup>Excellence Cluster ORIGINS, Boltzmannstrasse 2, D-85748 Garching, Germany
            <sup>42</sup>University Observatory, Faculty of Physics, Ludwig-Maximilians-Universität,
                             Scheinerstrasse 1, 81677 München, Germany
```

(Received 9 April 2025; accepted 12 August 2025; published 25 September 2025)

Recently the Dark Energy Spectroscopic Instrument (DESI) provided constraints on the expansion history from their Data Release 2. The DESI baryon acoustic oscillation measurements are well described by a flat  $\Lambda$ CDM model, but the preferred parameters are in mild (2.3 $\sigma$ ) tension with those determined from the cosmic microwave background. The DESI Collaboration has already explored a variety of solutions to this tension relying on variations in the late-time evolution of dark energy. Here we test an alternative—the introduction of an "early dark energy" (EDE) component. We find that EDE models can alleviate the tension, though they lead to differences in other cosmological parameters that have observational implications. Particularly the EDE models that fit the acoustic datasets prefer lower  $\Omega_m$ , higher  $H_0$ ,  $n_s$  and  $\sigma_8$  in contrast to the late-time solutions. We discuss the current status and near-future prospects for distinguishing amongst these solutions.

DOI: 10.1103/xtql-wh3h

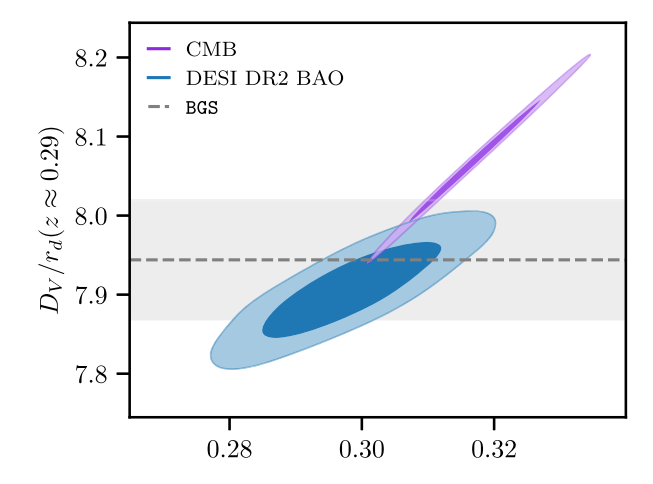
# I. INTRODUCTION

The measurement of the distance-redshift relation through baryon acoustic oscillations (BAO) in the second data release (DR2) of the Dark Energy Spectroscopic Instrument (DESI) Collaboration [1–4] has revealed a mild tension between acoustic waves measured in the cosmic microwave background (CMB) radiation and in BAO [5] when interpreted within the framework of ΛCDM. This tension has persisted for many years, over several experiments, and has been growing in significance (e.g., compare Fig. 1 to Fig. 12 of [6]). It is particularly puzzling, because BAO rely on a characteristic scale in the clustering of galaxies that arises from acoustic waves propagating in the coupled baryon-photon fluid in the prerecombination Universe (for a recent review see [7]; for textbook treatments see, e.g., [8,9]). This is the exact same physics as gives rise to the anisotropies in the CMB that have been exquisitely measured by WMAP [10], Planck [11] and a host of ground-based experiments, most recently Atacama Cosmology Telescope (ACT) [12–14] and SPO [15].

Individually the acoustic signals measured in the CMB and in DESI are each consistent with  $\Lambda$ CDM [5,10,11]; however there is a  $2.3\sigma$  tension<sup>1</sup> in the values of the cosmological parameters allowed by the two datasets; see [5]. Figure 1 shows the 68% and 95% marginal posteriors for  $\Omega_m$  and  $D_V/r_d$  at  $z \simeq 0.29$  and  $z \simeq 0.94$  from the CMB and BAO datasets described below. For the CMB the inference assumes the  $\Lambda$ CDM model, and the same is true of the BAO data but since this is very close to what the BAO natively constrain the model dependence of this

Contact author: echaussidon@lbl.gov

<sup>&</sup>lt;sup>1</sup>If we include CMB lensing. If not, the "tension" is  $2.0\sigma$  [5].



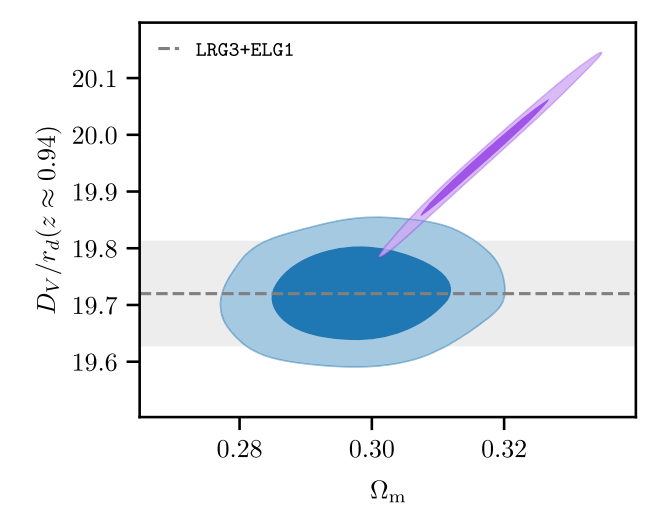


FIG. 1. The 68% and 95% marginal posteriors for  $\Omega_m$  and  $D_V/r_d$  at  $z\simeq 0.3$  and  $z\simeq 0.9$  from the CMB (purple) and BAO (blue) datasets are described in the text, within the context of  $\Lambda$ CDM. For the CMB we use the combination of Planck PR4 and Planck +  $\Lambda$ CT lensing [11], while for the BAO we use DESI DR2 [5]. The horizontal dashed line with shaded band is the central value and  $1\sigma$  error measured in DR2 for BGS at z=0.295 (top) and LRG3+ELG1 at z=0.934 (bottom); for reference, see Table 4 of [5]. The  $\Lambda$ CDM fit to the full DR2 dataset predicts distances in good agreement with the measured values at these redshifts while that fit to the CMB overpredicts these distances.

measurement is much weaker. Each dataset is individually consistent with  $\Lambda CDM$  but the "weak" tension rises when comparing the parameters preferred by each dataset within the  $\Lambda CDM$  paradigm.

If we assume the tension is not due to a statistical fluctuation or systematics in the measurements, then it can be resolved by changes to the model at low redshift (e.g., evolving dark energy) or between  $z \sim 10^4$  and  $10^3$  (e.g., "early" dark energy). Several late-time solutions are explored in Refs. [5,16,17]. In this paper we discuss a solution based on modifying the model at early times.

Specifically we study whether including an "early dark energy" (EDE) component that contributes to the expansion rate between matter-radiation equality and recombination can improve the agreement between high- and low-z measures of acoustic oscillations (i.e., the CMB and BAO). Other means of modifying the early-time expansion history are reviewed in [18]. The EDE component causes an increase in H(z) at early times, decreasing the acoustic scale. The adjustments in the other parameters (primarily an increase in  $H_0$  and slight lowering of  $\Omega_m$ ) to hold the well-measured acoustic scale of the CMB fixed allow a better fit with the DESI data.

The outline of this paper is as follows. In the next section (Sec. II) we describe the DESI data and the likelihoods that we employ. This is followed (Sec. III) by a discussion of the scalar field model that we use as an example of a modification of the expansion history at early times. Our fits and basic results are presented in Sec. IV. We then discuss the implications of these results for future measurements, and routes toward distinguishing between early-and late-time solutions, in Sec. V. Finally we conclude in Sec. VI.

## II. DATA AND COSMOLOGICAL INFERENCE

Our focus shall be on the two datasets that use the acoustic signature to provide cosmological constraints, specifically the CMB (from Planck and ACT) and BAO (from DESI). One of the advantages of the EDE model we shall discuss is that only the robust acoustic data are needed for data-driven (rather than prior dominated) constraints on the model. This is in contrast to solutions that modify the Dark Energy (DE) evolution at late times ( $w_0w_a$  model), where additional data (e.g., Type Ia SNe) are necessary.

We use the BAO measurements of the transverse  $(D_M)$  and line-of-sight  $(D_H)$  distances to seven redshift slices from DESI DR2 [19]. We follow common convention and define the combinations

$$D_V(z) = [zD_M^2(z)D_H(z)]^{1/3}$$
 (1)

$$F_{AP}(z) = D_M(z)/D_H(z),$$
 (2)

which measure the isotropically averaged distance to, and the anisotropy of the distances at, redshift z.

The DESI Collaboration used a robotic, 5000-fiber spectrograph [4,20–22] on the 4-m Nicholas U. Mayall Telescope at the Kitt Peak National Observatory to measure the redshifts [23,24] of galaxies and quasars with the goal of constraining cosmology via inhomogeneities in both galaxy density and the intergalactic medium [2]. In its first three years of operation DESI measured redshifts for over 30 million galaxies and quasars [25,26]. The DR2 dataset that we focus on, containing data taken between 14 May 2021 and 9 April 2024, uses  $\sim$ 14 million of these [19], plus the Ly $\alpha$  forest in the spectra of 820,000 QSOs [27], to

TABLE I. The priors used in our analysis. The parameter names have their usual meanings, or are defined in the text. The notation  $\mathcal{U}[a,b]$  indicates a uniform prior on the closed interval [a,b], while  $\mathcal{N}(\mu,\sigma)$  indicates a normal distribution with mean  $\mu$  and variance  $\sigma^2$ . We use the standard priors for the different nuisance parameters in the CMB likelihoods.

Parameter	Prior
$\Omega_m$	$\mathcal{U}[0.1, 0.9]$
$\omega_b$	$\mathcal{U}[0.021, 0.025]$
$H_0$	$\mathcal{U}[20, 100]$
$ln(10^{10}A_s)$	$\mathcal{U}[2.7, 3.3]$
$n_s$	$\mathcal{U}[0.9, 1.04]$
$ au_{ m reio}$	$\mathcal{U}[0.03, 0.1]$
$f_{ m EDE}$	$\mathcal{U}[0,0.3]$
$\log_{10}(a_c)$	$\mathcal{N}(-3.531, 0.1)$
$\Theta_{ m ini}$	$\mathcal{U}[0,\pi]$

measure BAO in seven redshift slices [5,28] spanning 0.1 < z < 3.5. Further information on the dataset, and the BAO methodology—which largely follows that used in DR1 [7,29–31]—can be found in Refs. [5,27,28].

Inclusion of the full information from the CMB is critical to constraining a model such as EDE. We follow Ref. [5] in using the temperature (TT), polarization (EE) and cross (TE) power spectra from Planck, specifically using the SIMALL, Commander (for  $\ell < 30$ ; [32]) and CamSpec (for  $\ell \geq 30$ ; [33]) likelihoods based upon the latest Planck release (NPIPE maps [34]). In addition to the primary anisotropies, we use the combination of Planck and ACT DR6 CMB lensing detailed in Ref. [12]. While there are several comparable choices of CMB likelihood, inferences about EDE are relatively insensitive to these choices [35,36] so we choose to follow those in Ref. [5].

For some of our results we shall also make use of SNe to constrain the low-z distance-redshift relation. We have chosen the Union3 sample [37] for illustrative purposes, and the choice of the SNe dataset does not impact our finding on EDE. In such cases we use "uncalibrated" SNe distances, i.e., marginalizing over an unknown absolute magnitude. The use of "calibrated" SNe for constraining  $H_0$  will be discussed later.

In the following, our cosmological inferences will be performed using DESILIKE.<sup>2</sup> The posterior profiling is performed through the IMINUIT [38] minimiser,<sup>3</sup> the Monte Carlo Markov chains use the EMCEE [39] sampler,<sup>4</sup> and we use GetDist [40] to display the posteriors. The priors

assumed in our analysis are given in Table I. For the latetime dark energy (i.e.,  $w_0w_a$ ) model we make use of the posteriors and the chains from Ref. [5], where they are described in some detail.

## III. EARLY DARK ENERGY

As shown in Fig. 1, the CMB data prefer a larger distance and a higher value of  $\Omega_m$  than do the BAO data. The same distance overprediction holds for all of the z < 1 distances constrained by DESI (see [5] or the second panel of Fig. 5). Interestingly this is the same direction as the offset predicted by the EDE model, so we expect EDE to alleviate some of this tension.

The specific example of an early-time modification to the expansion history that we shall study is the EDE model. This is usually realized as a canonically normalized, minimally coupled scalar field moving in a potential

$$V(\phi) = V_0 \left[ 1 - \cos \frac{\phi}{f} \right]^n, \qquad V_0 \equiv m^2 f^2 \qquad (3)$$

where  $f \sim M_{\rm Pl}$  is a decay constant,  $m \sim 10^{-28}$  eV a mass and  $n \approx 3$  for the model to be viable. We shall follow this practice as well, though we expect the arguments to be more general, and we shall fix n = 3 throughout. Rather than use m and f as our parameters, we shall follow the usual convention [35] and work with variables more closely related to the observations:  $\log_{10}(a_c)$  and  $f_{\rm EDE}$ . These are respectively the (logarithm of the) scale factor where the EDE density peaks and the fraction of  $\rho_{\rm crit}$  that it makes up at that time. We will see that  $a_c \sim 10^{-3.5}$  and  $f \sim 5-10\%$  will allow us to simultaneously fit the acoustic signatures in the CMB and DESI data with a single model. The final "additional" parameter in the EDE model is the initial value of the scalar field,  $\phi_i$ , which we will find prefers to be  $\Theta_i \equiv \phi_i / f \approx \pi$ . Note that in such situations the field evolves over the full potential range during cosmic evolution, in contrast to many scalar-fieldbased models of "late time" dark energy for which the field evolves very little.

The EDE model was originally proposed [41–43] to resolve the Hubble tension [44,45], but our goal is to use it as an example of a model that modifies the expansion history before recombination, and hence the sound horizon or "normalization" of the BAO ruler. A recent review of EDE models, and a comparison against current observations, can be found in Refs. [35,46], while [47] included the latest DESI DR1 BAO data.

The dynamics of the scalar field, and its fluctuations, can be straightforwardly computed [42,48,49], and we use the implementation of AxiCLASS<sup>5</sup> [43,50,51], based on CLASS

<sup>&</sup>lt;sup>2</sup>Publicly available: https://github.com/cosmodesi/desilike.

<sup>3</sup>https://github.com/cosmodesi/desilike/blob/main/desilike/profilers/minuit.py

<sup>&</sup>lt;sup>4</sup>https://github.com/cosmodesi/desilike/blob/main/desilike/samplers/emcee.py

<sup>&</sup>lt;sup>5</sup>We use AxiCLASS (https://github.com/PoulinV/AxiCLASS) via the PYTHON wrapper: https://github.com/cosmodesi/cosmoprimo.

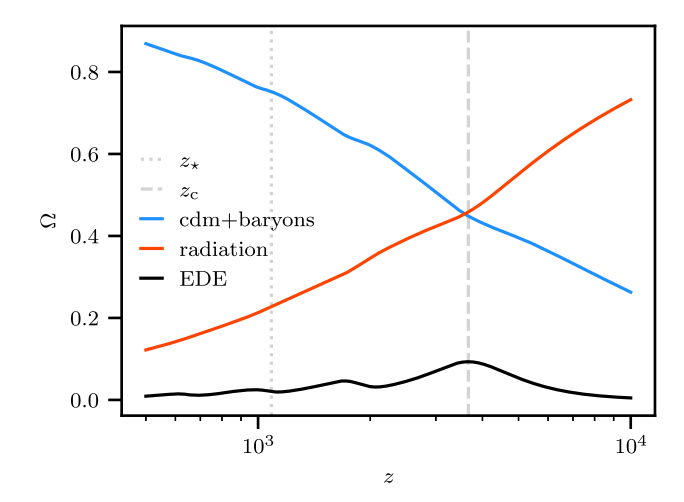


FIG. 2. Evolution of the energy densities in radiation (orange), matter (blue) and EDE (black) with redshift for our best-fitting EDE model, expressed as a fraction of the critical density. The EDE density peaks  $(z_c)$  near matter radiation equality  $(z_{eq})$  with an amplitude of 9.3% and is almost entirely gone by recombination  $(z_{\star})$ .

[52], to compute the background evolution and linear perturbations. To speed up the cosmological inference, we decide to emulate the required outputs of AxiCLASS with a neural network.<sup>6</sup>

At early times  $\phi$  is pinned by Hubble drag. It begins to act like a dark energy component when  $V(\phi) \sim H^2$ , at which point the field begins to roll down the potential and EDE becomes dynamical. As the field oscillates about the minimum of the potential,  $V(\phi) \propto \phi^{2n}$ , the EDE dilutes as an effective fluid with the equation of state, w = (n-1)/(n+1), i.e.,  $\rho_{\text{EDE}} \propto a^{-3(1+w)} \approx a^{-9/2}$ . Figure 2 shows the evolution of  $\rho_{\text{EDE}}$  for the model that best fits the data described in Sec. II.

The introduction of EDE allows us to hold the acoustic scale

$$\theta_{\star} = \frac{r_s}{\chi_{\star}}; \quad r_s = \int_{z_{\star}}^{\infty} \frac{c_s dz}{H(z)}, \qquad \chi_{\star} = \int_0^{z_{\star}} \frac{dz}{H(z)}$$
 (4)

fixed, while varying H(z) at both early and late times. In the above  $z_{\star} \approx 10^3$  is the redshift of last scattering. An increase in  $H(z > z_{\star})$ , from EDE, leads to a decrease in  $rac{7}{r_s}$ . Increasing  $H(z < z_{\star})$ , for example by increasing  $\omega_m$  or h, can compensate by decreasing  $\chi_{\star}$  to leave  $\theta_{\star}$  fixed, as required by the tight constraints from the

CMB. The field is required to decay quickly so that the diffusion damping scale<sup>8</sup> in the CMB [54] is not excessively modified.

# IV. RESULTS

Figure 3 shows the marginal likelihoods of several key cosmological parameters for the  $\Lambda \text{CDM}$ , EDE and  $w_0 w_a$  models when fit to the combination of CMB and BAO datasets, while Fig. 4 shows the marginal likelihoods of the EDE parameters and the impact on the most notable other cosmological parameters when fit to CMB, CMB+BAO and CMB + BAO + SNe datasets. Best fits and  $1\sigma$  confidence levels are given in Tables II and III. Both modifications to late-time DE dynamics and EDE induce shifts in the best-fit cosmological parameters (compared to  $\Lambda \text{CDM}$ ) in order to continue to fit the observations. In both cases the physical matter density  $(\omega_m)$  increases while  $\Omega_m$  decreases and  $H_0$  increases for EDE, and the opposite happens for  $w_0 w_a$ .

For EDE  $\omega_m$  increases due to the need to compensate for the EDE dynamics at  $z \sim z_c$  while holding  $\theta_{\star}$  fixed. Since the scalar field is "stiff," it contributes to the background expansion (H) but not to the potentials inside the horizon. It thus causes subhorizon modes to grow more slowly near matter-radiation equality and recombination. This can be compensated for by an increase in  $\omega_m$  in order to counteract the enhancement of the first acoustic peak in the CMB [55– 57]. To fix the spectrum at higher  $\ell$  the spectral index  $(n_s)$ also needs to increase, and there is a small increase in the normalization  $(A_s)$  [35,36] as shown in Fig. 4. The increase in  $\omega_m$  and h increases the expansion rate at low redshift,  $H(z) \propto \sqrt{h^2 + \omega_m e(z)} = h\sqrt{1 + \Omega_m e(z)}$  $e(z) = (1+z)^3 - 1$  for  $z \ll 100$ . This causes the required decrease in  $\chi_{\star}$  so that  $\theta_{\star}=r_{s}/\chi_{\star}$  is left unchanged even though  $r_s$  is decreased by 3% (measured in Mpc). We find H(z) is  $\approx 5\%$  higher over the range 0 < z < 1 in the bestfitting EDE model compared to the best-fitting ΛCDM model. The distances to  $z \ll 1$  are thus lowered modestly because  $H_0$  has increased. Since the majority of the change is through  $H_0$ , if distances are measured in  $h^{-1}$  Mpc then they change minimally. The quantity  $H_0r_d$ , being the BAO analog of  $\theta_{\star}$  in the CMB, is well constrained by BAO, and thus  $r_d$  is also almost unchanged in  $h^{-1}$  Mpc units.

For  $w_0w_a$  only the late-time dynamics is altered. Thus the drag scale  $(r_d)$  is unchanged, and the shift in  $\omega_m$  occurs so as to hold  $\chi_{\star}$ , and hence  $\theta_{\star}$ , fixed when the DE evolution at z < 1 is modified. The best-fitting model requires the dark energy to evolve quickly (in a fraction of the Hubble time) at late times, leading to a change in  $\chi(z)$  at z < 1 [5].

<sup>&</sup>lt;sup>6</sup>We use a multilayer perceptron whose implementation is available here: https://github.com/cosmodesi/cosmoprimo/blob/main/cosmoprimo/emulators/tools/mlp.py.

<sup>&</sup>lt;sup>7</sup>Although we shall distinguish between the sound horizon at recombination  $(r_s)$  and at the drag epoch  $(r_d)$  throughout, in fact for the models of interest  $r_d/r_s \approx 1.015$  is very close to constant.

<sup>&</sup>lt;sup>8</sup>Whereas the CMB acoustic scale,  $r_s$ , and the BAO acoustic scale,  $r_d$ , depend linearly on  $t_{\star}$ , the diffusion damping scale depends upon  $\sqrt{t_{\star}}$ . The combination of the two thus allows a constraint on early-time dynamics [53].

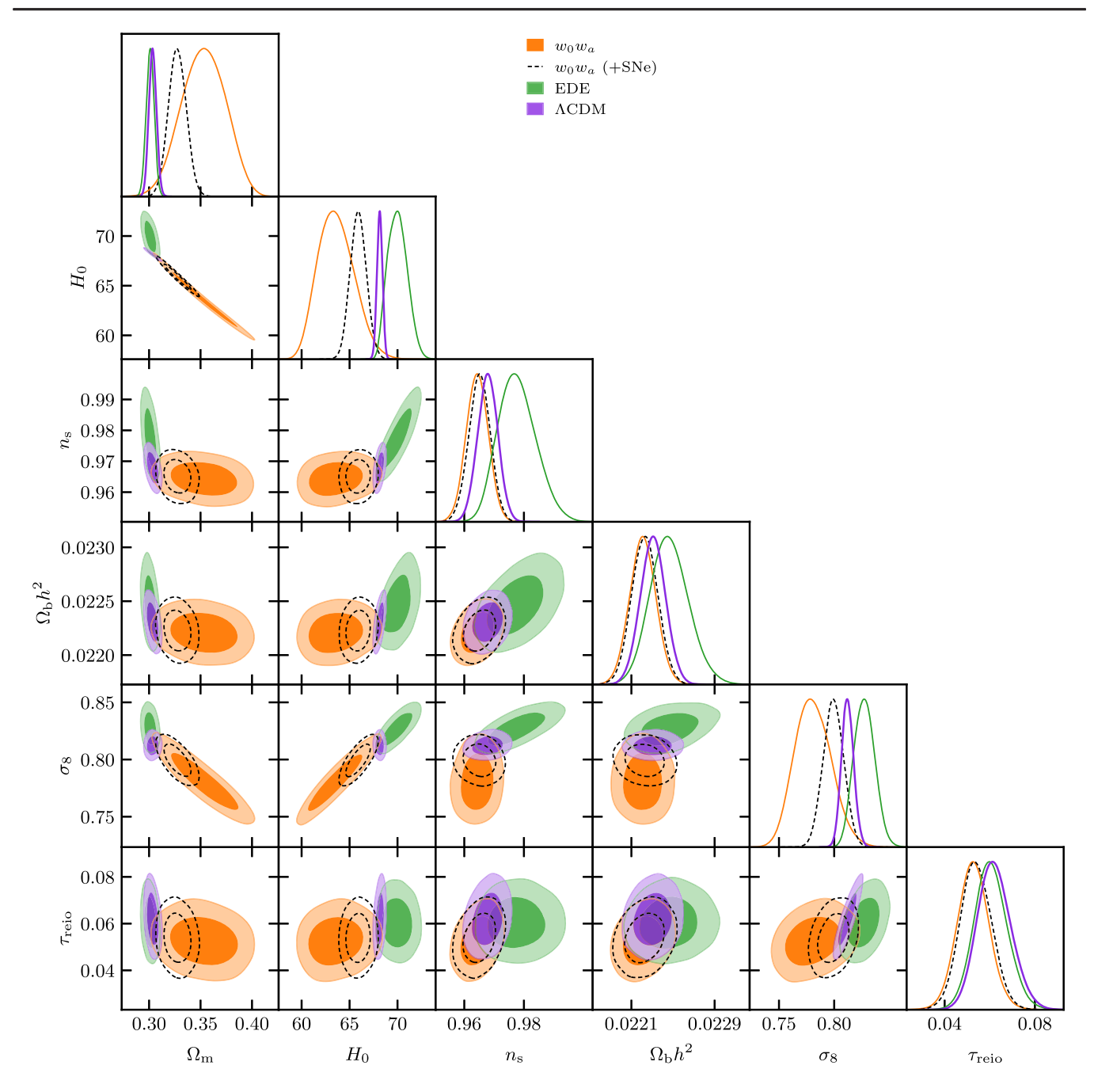


FIG. 3. Marginal 68% and 95% posteriors for the cosmological parameters in common to all models, for the combination of CMB and BAO data. Purple, green, and orange contours are for the  $\Lambda$ CDM, EDE and  $w_0w_a$  models, respectively, while the black dashed contour is the  $w_0w_a$  model including SNe (Unions3). Note the EDE model is consistent with higher values of  $H_0$ , and slightly smaller values of  $\Omega_m$ , than  $\Lambda$ CDM (as discussed in the text). The  $w_0w_a$  model shows the opposite trend.

In contrast to EDE, the late-time solution has a modest decrease in  $n_s$ ,  $A_s$  and  $\sigma_8$ .

While the constraints in Fig. 3 are superficially similar, the isotropic BAO distance  $(D_V/r_d)$  below  $z \simeq 1$  is smaller in the EDE model than the fiducial  $\Lambda$ CDM model fit to Planck, and in better agreement with the DESI BAO data, as shown in Fig. 5. By contrast  $F^{AP} = D_M/D_H$  is almost unchanged by the introduction of EDE, rather than following the data to increase toward lower z. However the

DESI constraints on  $F^{AP}$  are less stringent than on  $D_V/r_d$ , so this mismatch is not significant. The  $\Lambda$ CDM and EDE cases provide better agreement with the high-z data (i.e., the Ly $\alpha$  points), while the  $w_0w_a$  case does less well. The errors at high z are still sufficiently large, however, that this discrepancy is statistically insignificant.

Figure 6 shows the marginal posterior for  $H_0$  for our three models, fit to the acoustic datasets (CMB + BAO) for  $\Lambda$ CDM and EDE and with the inclusion of (uncalibrated)

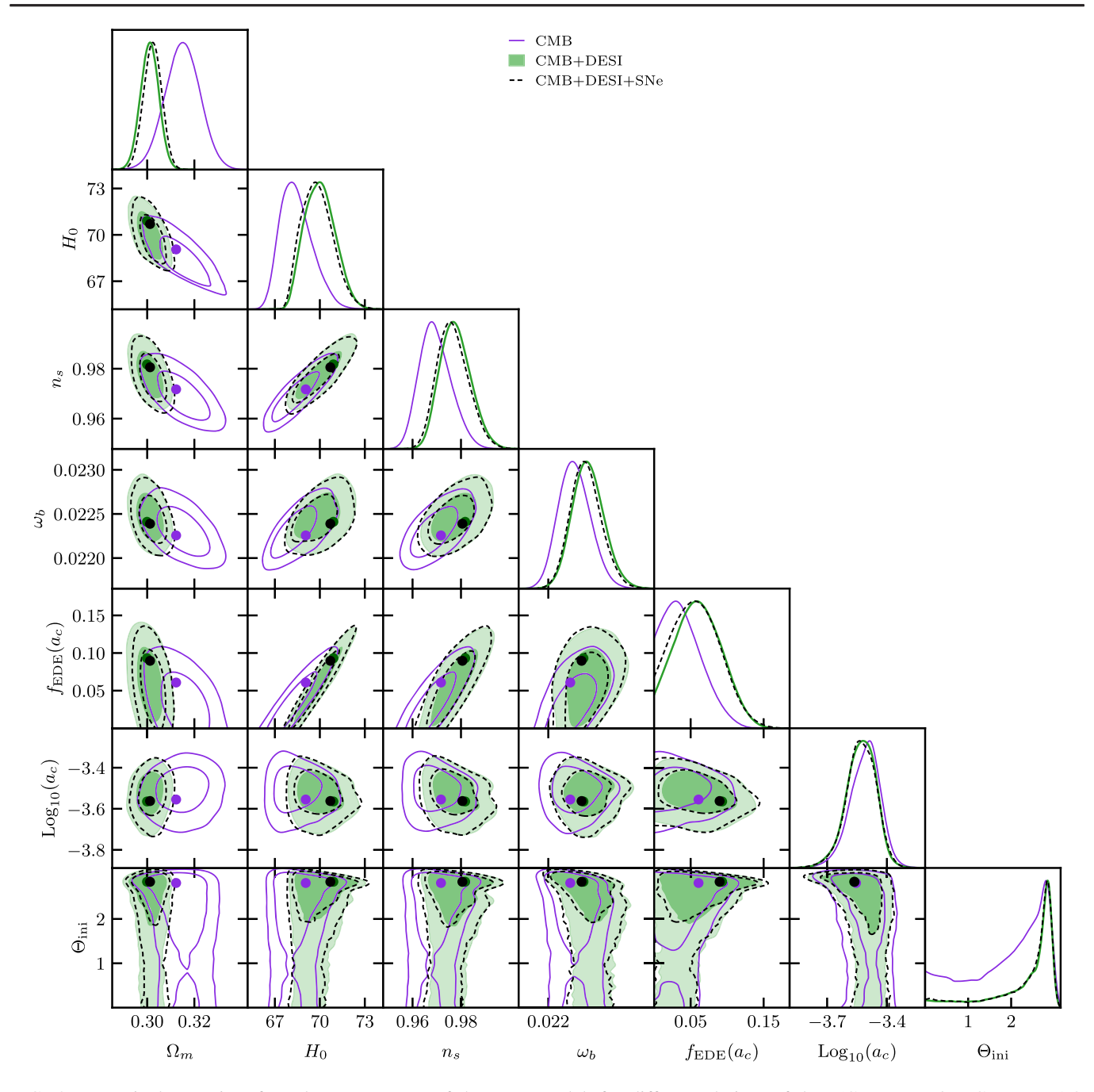


FIG. 4. Marginal posteriors for select parameters of the EDE model, for different choices of data (CMB [purple], CMB + BAO [green] and CMB + BAO + SNe [black]). Note that the model is well constrained by the CMB, but the parameters shift when the CMB data are combined with DESI BAO. The parameters remain stable under the addition of SNe data (Union3). When low- and high-z data are included the model prefers lower  $\Omega_m$  and higher  $H_0$  than with CMB alone. The solid dots are the Maximum A Priori (MAP) for the different choices of data, indicating no serious parameter projection effects for any data combination.

SNe from Union3 for the  $w_0w_a$  model. The inferences from the distance ladder by the SH0ES [58] and CCHP [59] teams are shown as vertical bands. As has been noted previously [35,36,46] EDE models consistent with CMB have their most probable values below the SH0ES result on  $H_0$ , though the tension is lessened compared to  $\Lambda$ CDM. The  $w_0w_a$  models fare even more poorly in this regard.

However the CCHP result is consistent with the predictions of all three of our models, though only marginally for  $w_0w_a$ . Since the  $H_0$  value allowed by the combination of CMB and BAO within the EDE model is higher than within  $\Lambda$ CDM it overlaps considerably with that inferred by CCHP. If we include the  $H_0$  values in our fits then the preference for EDE over  $\Lambda$ CDM or  $w_0w_a$  improves (see

Constraints on the parameters of the different models for each of the data combinations considered in this analysis. The central values are the best fit values from the IMINUIT minimization while the errors are the  $1\sigma$  credible interval from the corresponding chains. The last column shows the  $\Delta\chi^2$  difference of the MAP points for each model. For ACDM and EDE models, the  $\chi^2$  is computed without the emulator at the best fit found with the emulator. Additional parameters are given in Table III.

Data (Model)	$\Omega_m$	$H_0$	$\sigma_8$	$f_{ m EDE}$	$\log_{10}(a_c)$	$\mathcal{W}_0$	$W_a$
CMB (ACDM)	$0.3188 \pm 0.0067$	$67.02 \pm 0.48$	$0.8122 \pm 0.0052$	:	:	:	:
$CMB + DESI (\Lambda CDM)$	$0.3037 \pm 0.0037$	$68.12 \pm 0.28$	$0.8101 \pm 0.0055$	:	:	:	:
CMB + DESI (EDE)	$0.2999 \pm 0.0038$	$70.9 \pm 1.0$	$0.8283 \pm 0.0093$	$0.093 \pm 0.031$	$-3.564 \pm 0.075$	:	:
$\mathrm{CMB} + \mathrm{DESI}\left(w_0 w_a\right)$	$0.353 \pm 0.021$	$63.5\pm1.9$	$0.780 \pm 0.016$	:	:	$-0.42 \pm 0.21$	$-1.75 \pm 0.58$
CMB + DESI + SNe (ACDM)	$0.3047 \pm 0.0036$	$68.04 \pm 0.28$	$0.8102 \pm 0.0054$	:	:	:	:
CMB + DESI + SNe (EDE)	$0.3012 \pm 0.0037$	$70.7 \pm 1.0$	$0.8277 \pm 0.0097$	$0.09 \pm 0.032$	$-3.562 \pm 0.077$	:	:
$\mathrm{CMB} + \mathrm{DESI} + \mathrm{SNe}\left(w_0w_a\right)$	$0.3270 \pm 0.0086$	$65.92 \pm 0.84$	$0.7989 \pm 0.0093$	:	:	$-0.672 \pm 0.088$	$-1.06 \pm 0.29$

As in Table II but for the "base" ACDM parameters. The central values are the best fit value from the IMINUIT minimization while the errors are the 1 $\sigma$  credible interval from the corresponding chains. TABLE III.

Data (Model)	$\omega_m$	$H_0$	$n_s$	$\omega_b$	$\ln{(10^{10}A_s)}$	$ au_{ m reio}$
CMB (ACDM)	$0.1432 \pm 0.0010$	$67.02 \pm 0.48$	$0.9593 \pm 0.0039$	$0.02212 \pm 0.00013$	$3.044 \pm 0.013$	$0.0547 \pm 0.0073$
CMB + DESI (ACDM)	$0.1409 \pm 0.00061$	$68.12 \pm 0.28$	$0.9672 \pm 0.0034$	$0.02229 \pm 0.00012$	$3.056 \pm 0.014$	$0.0621 \pm 0.0075$
CMB + DESI (EDE)	$0.1507 \pm 0.0035$	$70.9 \pm 1.0$	$0.9817 \pm 0.0063$	$0.02241 \pm 0.00018$	$3.067 \pm 0.017$	$0.0582 \pm 0.0074$
$\operatorname{CMB} + \operatorname{DESI}\left(w_0w_d\right)$	$0.142 \pm 0.021$	$63.5\pm1.9$	$0.9632 \pm 0.0037$	$0.02218 \pm 0.00013$	$3.037 \pm 0.013$	$0.0520 \pm 0.0071$
CMB + DESI + SNe (ACDM)	$0.1410 \pm 0.00060$	$68.04 \pm 0.28$	$0.9668 \pm 0.0033$	$0.02228 \pm 0.00012$	$3.055 \pm 0.013$	$0.0605 \pm 0.0073$
CMB + DESI + SNe (EDE)	$0.1505 \pm 0.0036$	$70.7 \pm 1.0$	$0.9806 \pm 0.0064$	$0.02239 \pm 0.00018$	$3.066 \pm 0.014$	$0.0578 \pm 0.0073$
$\mathrm{CMB} + \mathrm{DESI} + \mathrm{SNe}\left(w_0w_a\right)$	$0.1421 \pm 0.0086$	$65.92 \pm 0.84$	$0.9646 \pm 0.0036$	$0.02221 \pm 0.00013$	$3.039\pm0.013$	$0.0529 \pm 0.0070$

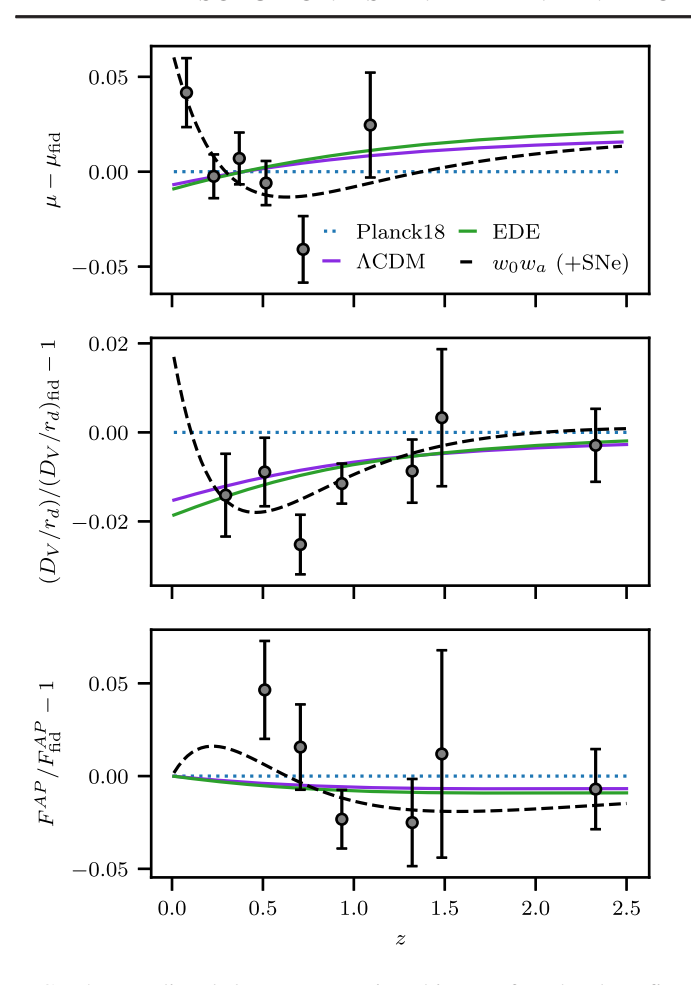


FIG. 5. Predicted low-z expansion history for the best-fit models. In each panel the purple, green and black lines are the predictions of the  $\Lambda$ CDM, EDE and  $w_0wa$  models that best fit the combination of CMB + BAO data discussed in the text, compared to the DESI "fiducial"  $\Lambda$ CDM model (also used as the fiducial cosmology in Ref. [5]). The top panel shows the distance modulus, such as would be measured by SNe, the middle panel the isotropic distance scale constrained by BAO and the lower panel the distance ratio. The points with error bars in the top panel are binned data from the Union3 SNe dataset, with the weighted mean set to zero to account for the unknown absolute magnitude. The points in the middle and lower panel are from DESI DR2. Note that  $\Lambda$ CDM and EDE predict similar late-time expansion, but the  $\Lambda$ CDM model provides a worse fit to the data combination than the EDE model (Table IV).

Table IV). New data and improved analysis methods [60,61] are already reducing the systematic errors in the local distance scale, and will help to resolve this discrepancy between the two  $H_0$  measures.

To compare the different models, we show<sup>9</sup> in Table IV the  $\chi^2_{\text{MAP}}$  at the best fit parameters. The best fit for  $w_0w_a$  is taken from Ref. [5]. Note that we found a slightly larger

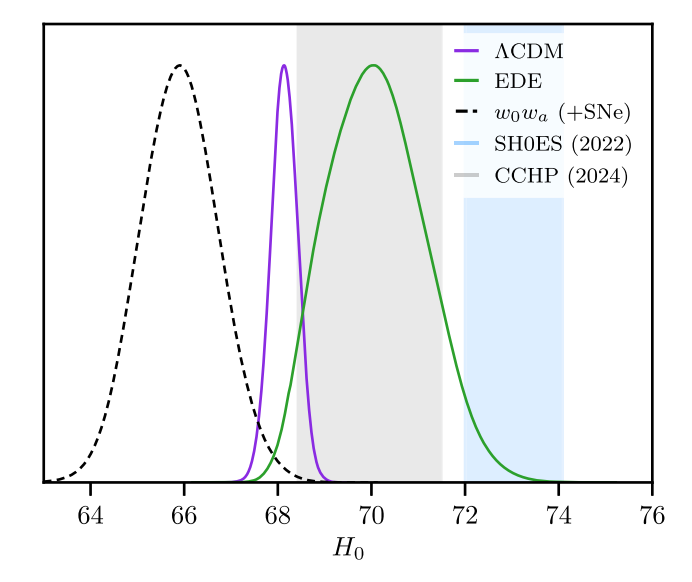


FIG. 6. The  $H_0$  posteriors for our three models fit to the combination of CMB + BAO data, including + SNe (Union3) for the  $w_0w_a$  model. The values inferred from the local distance ladder by the SH0ES and CCHP teams are shown as vertical bands.

 $\Delta\chi^2_{\rm MAP}$  for  $w_0w_a$  over  $\Lambda{\rm CDM}$  than quoted in Ref. [5]. This is because we are computing the  $\chi^2_{\rm MAP}$  for  $\Lambda{\rm CDM}$  at the best fit found by our emulator instead of the best fit found in [5], resulting in a difference of about  $\Delta\chi^2 \sim 1$ . Finally, we speculate that the residual small mismatch between our computation using CLASS and that of Ref. [5] using CAMB may be resolved by increasing the accuracy settings in CLASS.

Regardless of these details, we find that, for CMB+BAO, the addition of EDE improves the fit over the  $\Lambda$ CDM model by  $\Delta \chi^2_{\text{MAP}} = 7.4$ , close to a  $2\sigma$ 

TABLE IV. Relative goodness of fit of the models in Tables II and III (and discussed in the text) for various dataset combinations. For each data combination we quote the  $\chi^2$  difference at the MAP point,  $\Delta\chi^2_{\rm MAP}$ , between  $\Lambda{\rm CDM}$  and the EDE model and between the  $\Lambda{\rm CDM}$  and  $w_0w_a$  model. The term "SNe" refers to "uncalibrated" SNe to measure the distance-redshift relation while CCHP and SH0ES refer to the "calibrated" distance ladder (including SNe). A positive number indicates a preference over  $\Lambda{\rm CDM}$ . Note that for simplicity when including CCHP or SH0ES we simply report  $\Delta\chi^2_{\rm MAP}$  for the models already described rather than refitting to the combined data.

Data	ΛCDM—EDE	$\Lambda$ CDM $-w_0w_a$
CMB + BAO	7.4	13
+SNe	7.5	19
+CCHP	8.7	-2.9
+SH0ES	25	-48.5
+SNe + CCHP	8.7	14
+SNe + SH0ES	26	-4.6

<sup>&</sup>lt;sup>9</sup>We use our emulators to find the best fits shown in Table II, but then compute  $\chi^2$  at the best fit parameters, with AxiCLASS without using our emulator.

improvement given the 3 additional degrees of freedom. As expected, the inclusion of (uncalibrated) SNe data does not further increase  $\Delta\chi^2_{\rm MAP}$  as the EDE model does not match the evolution desired by the SNe. By comparison, for the same data, late-time evolving dark energy improves the  $\chi^2_{\rm MAP}$  by 13.2 using only two new parameters. This increases to 19 when we include the SNe data, since a rapidly evolving late-time dark energy can better fit the SNe data below  $z \simeq 0.5$ . If we add measures of  $H_0$  from the local distance scale, then the relative preference for  $w_0w_a$  over EDE is reduced (see Table IV), since the  $w_0w_a$  models reduce  $H_0$  while the EDE models increase it.

# V. IMPLICATIONS FOR FUTURE MEASUREMENTS

Almost by design, the EDE model<sup>10</sup> shifts the sound horizon while leaving the shape of the late-time expansion history unchanged from ACDM. As Fig. 5 shows, this allows us to provide a good match to the BAO data (second and third panels) while simultaneously matching the CMB. However it does not provide as good a fit to the rapid increase in  $\mu - \mu_{fid}$  at low z preferred by the "uncalibrated" SNe data, as displayed in the first panel of Fig. 5 and shown in the first two rows of Table IV (the case of Union3 [37] is shown in Fig. 5; the data from DES Y5 [62] appear similar while the tendency is less pronounced in the Pantheon+ [63] dataset). We expect further improvements to the SNe data with ongoing and upcoming surveys [64,65], and improvements in the low-z BAO measurements by extending the footprint of DESI; these measurements will be highly informative regarding the viability of an early-time solution to the current tension. If the BAO, even used as an uncalibrated ruler, show a similar behavior to the SNe (see the first two panels of Fig. 5) then an EDE solution will be (more) disfavored since it will not be able to produce this behavior.

Any component that alters the expansion history and evolution of the perturbations at  $z\approx 10^3$  risks destroying the good agreement between observations and theoretical models of the CMB anisotropy. In particular, the E mode of the CMB anisotropy polarization power spectrum ( $C_\ell^{EE}$ ) is very sensitive to these effects. Figure 7 shows the ratio of  $C_\ell^{EE}$  in our best-fitting, evolving DE cosmologies (Table II) to that of the best-fitting  $\Lambda$ CDM cosmology. The gray bands indicate the forecasted  $1\sigma$  errors from future measurements by the Simons Observatory [66,67]. Although the differences are very small, the fraction of EDE preferred by the current CMB + BAO data ( $f_{\rm EDE}\approx 0.09$ ) could be confirmed or ruled out by this new CMB dataset.

Figure 8 compares the linear theory, matter power spectrum at z = 1 for the best-fitting  $\Lambda$ CDM model,

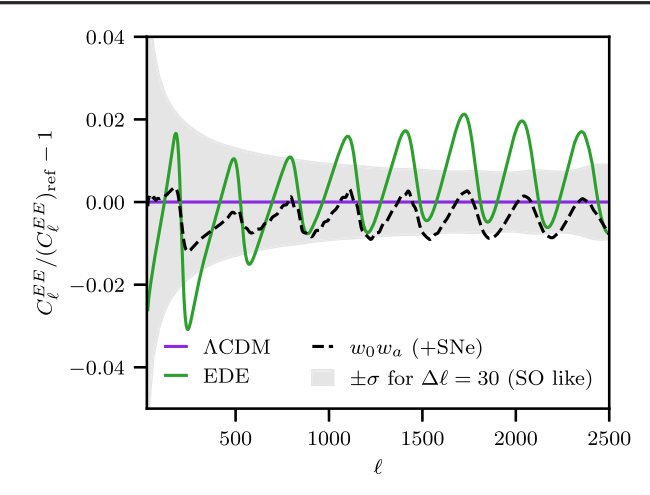


FIG. 7. *E*-mode polarization autospectrum between the best fit EDE model for the combination of CMB + BAO data (green line) and  $w_0w_a$  model for the combination CMB + BAO + SNe with Union3 (black dashed line) as the ratio with respect to the best fit  $\Lambda$ CDM model for CMB + BAO. The gray band is the expected  $1\sigma$  errors with  $\Delta\ell=30$  for a measurement by an instrument similar to the Simons Observatory.

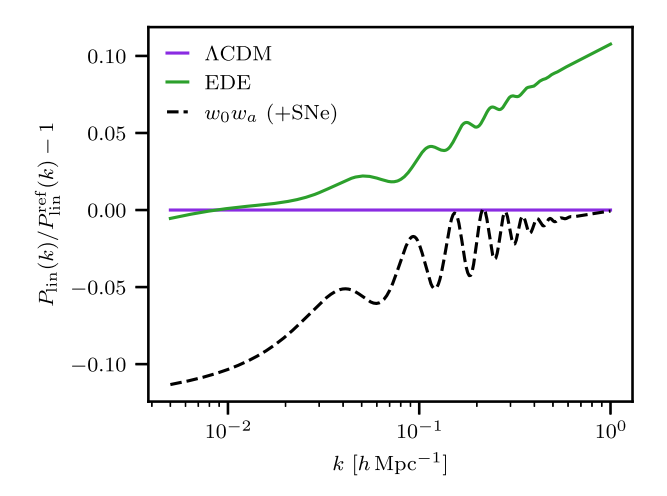


FIG. 8. Ratio of the linear matter power spectrum at z=1 between our three model best fits to the combination of BAO + CMB data, plus SNe (Union3) for the  $w_0w_a$  model. We have chosen the  $\Lambda$ CDM model as the reference.

 $w_0w_a$  model<sup>11</sup> and our best-fitting EDE model (the associated  $\sigma_8$  values are given in Table II). The fact that the best-fitting EDE model predicts a higher amplitude of clustering at late times than the best-fitting  $\Lambda$ CDM model has been noted (and explained) before, and has been used to disfavor

<sup>&</sup>lt;sup>10</sup>We do not consider a combination of early- and late-time evolving dark energy in this paper.

<sup>&</sup>lt;sup>11</sup>Since we do not have a "microphysical" model for the  $w_0w_a$  case, we compute the power spectra within the parametrized post-Friedman approximation, so the results assume the validity of that approximation. However at  $z \simeq 1$  the impact of dark energy is still small, so we believe this to be a reasonable approach.

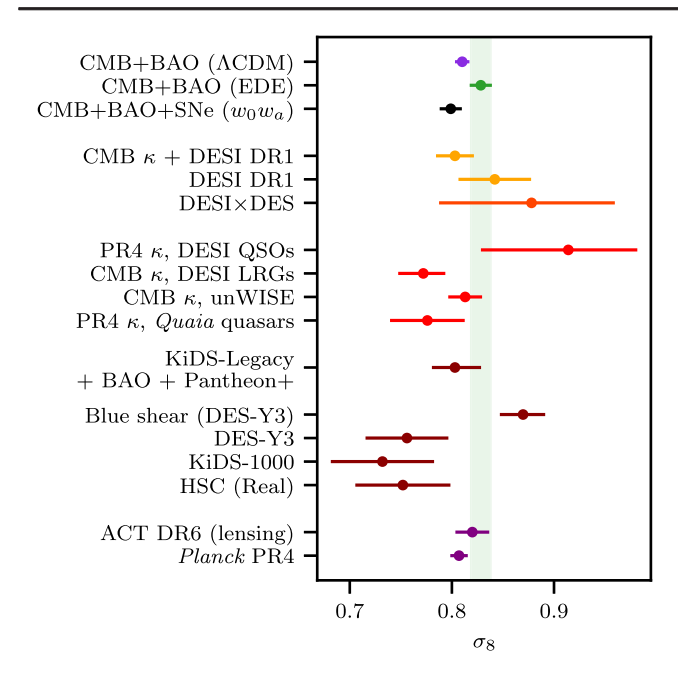


FIG. 9. A selection of recent measurements of the low-z amplitude of the power spectrum. The top points show the measurements from this paper; other measurements are taken from the literature (see text for citations). We caution the reader that most of these constraints are done outside the context of EDE models, and the redshifts and scales probed differ significantly so the points should be taken as indicative. For the cosmic shear datasets, we have converted from  $S_8$  to  $\sigma_8$  where necessary using their best fit  $\Omega_m$ , i.e., assuming motion along the degeneracy is largely unconstrained.

the EDE model [35,46,56,68,69]. While such a prediction increases the " $S_8$ -tension" [45] we note that there have been some new results that bear upon this issue (Fig. 9 shows a compilation of recent measurements [70-82] compared to our theoretical predictions). The 3D clustering amplitude inferred from modern perturbation theory models fit to the DESI data is larger than when these same class of models are fit to the older BOSS data [81]. New investigations into modeling assumptions within weak lensing surveys [74,75,80,83–88] have also suggested that larger clustering amplitudes may be allowed by those data than previously thought. Similarly, newer measurements of the CMB lensing autospectrum [13] are consistent with clustering amplitudes on the "high end" of the range. For these reasons, we regard the prediction of EDE models for higher clustering to be concerning but provisionally allowed, pending a new analysis that self-consistently includes the impact of EDE.

Fortunately, new data will enable us to perform a precise test of this model in the very near future. Wide-area cosmic shear catalogs are becoming available [89], cosmology analysis of the final release of the Dark Energy Survey [90] is imminent, Euclid [91] is in orbit and expected to return data soon and the Legacy Survey of Space and Time on the Vera Rubin Observatory [65] will begin in short order.

Perhaps the strongest constraints will come from DESI DR2 data. Both the volume surveyed and the completeness of the DESI survey have improved dramatically compared to the DR1 data described above [81], enabling a 3D clustering analysis in which theoretical assumptions can be tightly controlled while still returning tight constraints. Within the context of modern perturbation theory treatments, most cosmological constraining power comes from  $k < 0.1h~{\rm Mpc^{-1}}$ , with nuisance parameters degrading the impact of higher-k terms. The effective volume for DR2 is  $2.2 \times$  times larger than for DR1, suggesting differences such as those in Fig. 8 should be distinguishable. We intend to return to this question once the relevant data are unblinded within the DESI Collaboration.

Finally we note that within the EDE model the changes to the power spectrum shape affect a wide range of redshifts. Therefore high z measures at smaller scales, from the Ly $\alpha$  forest [92,93] or future spectroscopic surveys [94,95] for example, could potentially provide even stronger constraints on (or support for) the model. We leave any such investigation to future work.

## VI. CONCLUSIONS

The recent DR BAO results from DESI [5] have increased the significance of the long-standing tension between acoustic waves measured in the CMB and BAO when interpreted within the ACDM model. While still of modest statistical significance  $(2.3\sigma)$  it lends support to other lines of evidence arguing for a revision of the standard cosmological model (see [5] for further discussion). References [5,16,17] explored solutions to this puzzle that alter the behavior of DE at late times. In this paper we have investigated solutions that instead alter the dynamics at high redshift. As a specific example, we have studied the impact of EDE in the form of a scalar field whose energy density contributes  $\mathcal{O}(10\%)$  of the critical density at  $z \sim 10^{3-4}$  before rapidly redshifting away. Such a field briefly alters the expansion history, and thus the sound horizon scale that sets the "standard ruler" for BAO.

Our main focus has been on cosmological probes based on acoustic oscillations in the early and late Universe, specifically the CMB and BAO. For the former we concentrate on Planck PR4 (including CMB lensing from Planck and ACT), while for the latter we use the newly released DESI DR2 BAO measurements. While we discuss the inclusion of SNe data, it turns out that the acoustic datasets alone provide enough information to constrain the parameters of the EDE model (in contrast to the situation with the late-time model exemplified by  $w_0w_a$ ).

We find that an EDE model can modestly ( $\Delta\chi^2_{\rm MAP}=7.4$  for three additional parameters) improve the agreement between the two key acoustic physics observables: the CMB and BAO. Within the  $\Lambda$ CDM model the CMB data prefer larger distances to  $z\simeq 0.3-1$  and a higher value of  $\Omega_m$  than do the BAO data. For dark energy fractions of

 $\approx 10\%$  the EDE model resolves these discrepancies, reducing the sound horizon at the drag epoch  $(r_d)$  by 3% and increasing H(z<10) by  $\approx 5\%$ . This allows a model with  $\Omega_m \simeq 0.3$  and  $h \simeq 0.7$  to provide simultaneously good fits to the CMB and BAO data. The final parameters are relatively close to those of the  $\Lambda$ CDM model fit to the same data combination, but in that case the two datasets are in (mild) tension and the agreement is more of a compromise on a model that neither set particularly prefers.

The set of EDE models that fit the combination of CMB and BAO data have higher  $\omega_m$  and  $H_0$  but lower  $\Omega_m$  than  $\Lambda$ CDM. The shift in  $H_0$  is larger than in  $\Omega_m$  such that H(z) is increased by  $\approx 5\%$  over the range 0 < z < 1. If distances are measured in  $h^{-1}$ Mpc, to incorporate this shift in  $H_0$ , then the distance scale is largely unchanged by the introduction of EDE. By contrast the late-time solutions prefer higher  $\Omega_m$  and lower  $H_0$  (though  $\omega_m$  is also modestly increased in this model). The expansion history at low z is altered much more significantly than in the EDE model.

Both the best-fitting EDE model and the best-fitting  $w_0w_a$  model feature a dark energy component that first rises and then decays with cosmic time. For both models the rise and decay take place over  $\approx 1$  e-fold in expansion. For EDE the DE component is never dominant, making up at most 10% of the total energy density (Fig. 2). For the  $w_0w_a$  model that best fits the CMB + BAO + SNe data  $H^{-1}d\ln\rho_{\rm DE}/dt$  runs from  $\approx 2$  at early time to  $\approx -1$  today. Naively extrapolating into the future,  $\rho_{\rm DE} > \rho_m$  for just under 1.5 e-folds of expansion. Of course in the  $w_0w_a$  model the action is near to the present day while for EDE it is confined to a few hundred thousand years after the big bang. The EDE model additionally requires a cosmological constant component in order to match the accelerated expansion of the Universe today.

Assuming that we are not being misled by a statistical fluke or erroneous data, the emerging "acoustic tension" suggests a solution either in the early- or late-time Universe. At present both are allowed by the data, but they make different predictions that allow them to be observationally distinguished. For example, two of the SNe datasets prefer a late-time solution, with a rapid evolution in the dark energy below  $z \simeq 0.5$ . Newer SNe data and improved BAO measurements from increased sky coverage will help to sharpen this distinction. The values of  $H_0$  in the EDE model are larger than in  $\Lambda$ CDM while those in  $w_0 w_a$  are smaller. Improved distance-scale measurements will provide further discrimination. The EDE models predict very modestly lower  $\Omega_m$  than  $\Lambda$ CDM, while  $w_0 w_a$ prefers higher values. At the level of the perturbations, both the CMB and future large-scale structure data could definitively settle this issue because the different models predict quite different CMB anisotropies and clustering. In fact, the EDE model is already under tension from existing large-scale structure datasets, and DESI DR2 should provide significantly improved constraints in this regard.

While this work was under collaboration review within DESI, the ACT Collaboration released their latest results [96,97]. The mismatch in  $\Omega_m$  between CMB and BAO, when interpreted within the  $\Lambda$ CDM framework, persists in the data [96] though it is slightly lessened in the combination of Planck and ACT. The ACT data also allow  $f_{\rm EDE}$  at the levels required to resolve the acoustic tension between CMB and BAO [97]. The constraints tighten significantly if likelihoods preferring a lower clustering amplitude are included, but as we have argued above the strength of this tension is currently under debate within the community.

## ACKNOWLEDGMENTS

This material is based upon work supported by the U.S. Department of Energy (DOE), Office of Science, Office of High-Energy Physics, under Contract No. DE-AC02-05CH11231, and by the National Energy Research Scientific Computing Center, a DOE Office of Science User Facility under the same contract. Additional support for DESI was provided by the U.S. National Science Foundation (NSF), Division of Astronomical Sciences under Contract No. AST-0950945 to the NSF's National Optical-Infrared Astronomy Research Laboratory; the Science and Technology Facilities Council of the United Kingdom; the Gordon and Betty Moore Foundation; the Heising-Simons Foundation; the French Alternative Energies and Atomic Energy Commission (CEA); the National Council of Humanities, Science Technology of Mexico (CONAHCYT); the Ministry of Science, Innovation and Universities of Spain (MICIU/ AEI/10.13039/501100011033), and by the DESI Member Institutions: [98].

Any opinions, findings, and conclusions or recommendations expressed in this material are those of the author(s) and do not necessarily reflect the views of the U.S. National Science Foundation, the U.S. Department of Energy, or any of the listed funding agencies. The authors are honored to be permitted to conduct scientific research on I'oligam Du'ag (Kitt Peak), a mountain with particular significance to the Tohono O'odham Nation.

# DATA AVAILABILITY

The data that support the findings of this article are openly available [99].

- [1] M. Levi, C. Bebek, T. Beers, R. Blum, R. Cahn, D. Eisenstein *et al.*, The DESI Experiment, a whitepaper for Snowmass 2013, arXiv:1308.0847.
- [2] A. Aghamousa, J. Aguilar, S. Ahlen, S. Alam, L. E. Allen *et al.* (DESI Collaboration), The DESI experiment part I: Science, targeting, and survey design, arXiv:1611.00036.
- [3] A. Aghamousa, J. Aguilar, S. Ahlen, S. Alam, L. E. Allen *et al.* (DESI Collaboration), The DESI experiment part II: Instrument design, arXiv:1611.00037.
- [4] B. Abareshi, J. Aguilar, S. Ahlen, S. Alam, D. M. Alexander et al. (DESI Collaboration), Overview of the instrumentation for the Dark Energy Spectroscopic Instrument, Astron. J. 164, 207 (2022).
- [5] DESI Collaboration, DESI DR2: Measurements of baryon acoustic oscillations and cosmological constraints, arXiv: 2503.14738.
- [6] N. Aghanim, Y. Akrami, M. Ashdown, J. Aumont, C. Baccigalupi *et al.* (Planck Collaboration), Planck 2018 results. VI. Cosmological parameters, Astron. Astrophys. 641, A6 (2020).
- [7] S. F. Chen, C. Howlett, M. White, P. McDonald, A. J. Ross, H. J. Seo *et al.*, Baryon acoustic oscillation theory and modelling systematics for the DESI 2024 results, Mon. Not. R. Astron. Soc. **534**, 544 (2024).
- [8] S. Dodelson and F. Schmidt, Modern Cosmology (Academic Press, New York, 2020).
- [9] D. Huterer, *A Course in Cosmology* (Cambridge University Press, Cambridge, England, 2023).
- [10] C. L. Bennett, D. Larson, J. L. Weiland, N. Jarosik, G. Hinshaw, N. Odegard *et al.*, Nine-year Wilkinson Microwave Anisotropy Probe (WMAP) observations: Final maps and results, Astrophys. J. Suppl. Ser. 208, 20 (2013).
- [11] N. Aghanim, Y. Akrami, F. Arroja, M. Ashdown, J. Aumont *et al.* (Planck Collaboration), Planck 2018 results. I. Overview and the cosmological legacy of Planck, Astron. Astrophys. **641**, A1 (2020).
- [12] M. S. Madhavacheril, F. J. Qu, B. D. Sherwin, N. MacCrann, Y. Li, I. Abril-Cabezas *et al.*, The Atacama Cosmology Telescope: DR6 gravitational lensing map and cosmological parameters, Astrophys. J. 962, 113 (2024).
- [13] F. J. Qu, B. D. Sherwin, M. S. Madhavacheril, D. Han, K. T. Crowley, I. Abril-Cabezas *et al.*, The Atacama Cosmology Telescope: A measurement of the DR6 CMB lensing power spectrum and its implications for structure growth, Astrophys. J. **962**, 112 (2024).
- [14] N. MacCrann, B. D. Sherwin, F. J. Qu, T. Namikawa, M. S. Madhavacheril, I. Abril-Cabezas *et al.*, The Atacama Cosmology Telescope: Mitigating the impact of extragalactic foregrounds for the DR6 cosmic microwave background lensing analysis, Astrophys. J. **966**, 138 (2024).
- [15] R. Chown, Y. Omori, K. Aylor, B. A. Benson, L. E. Bleem, J. E. Carlstrom *et al.*, Maps of the southern millimeter-wave sky from combined 2500 deg<sup>2</sup> SPT-SZ and Planck temperature data, Astrophys. J. Suppl. Ser. **239**, 10 (2018).
- [16] K. Lodha et al., Extended Dark Energy analysis using DESI DR2 BAO measurements, arXiv:2503.14743.
- [17] W. Elbers *et al.*, Constraints on Neutrino Physics from DESI DR2 BAO and DR1 Full Shape, arXiv:2503.14744.
- [18] T. L. Smith and N. Schöneberg, Predictions for new physics in the CMB damping tail, arXiv:2503.20002.

- [19] DESI Collaboration, DESI DR2: Data release 2 of the Dark Energy Spectroscopic Instrument (to be published).
- [20] J. H. Silber, P. Fagrelius, K. Fanning, M. Schubnell, J. N. Aguilar, S. Ahlen *et al.*, The robotic multiobject focal plane system of the Dark Energy Spectroscopic Instrument (DESI), Astron. J. **165**, 9 (2023).
- [21] C. Poppett, L. Tyas, J. Aguilar, C. Bebek, D. Bramall, T. Claybaugh *et al.*, Overview of the fiber system for the Dark Energy Spectroscopic Instrument, Astron. J. **168**, 245 (2024).
- [22] T. N. Miller, P. Doel, G. Gutierrez, R. Besuner, D. Brooks, G. Gallo *et al.*, The optical corrector for the Dark Energy Spectroscopic Instrument, Astron. J. **168**, 95 (2024).
- [23] J. Guy, S. Bailey, A. Kremin, S. Alam, D. M. Alexander, C. Allende Prieto *et al.*, The spectroscopic data processing pipeline for the Dark Energy Spectroscopic Instrument, Astron. J. 165, 144 (2023).
- [24] Bailey et al. (to be published).
- [25] A. D. Myers, J. Moustakas, S. Bailey, B. A. Weaver, A. P. Cooper, J. E. Forero-Romero *et al.*, The target-selection pipeline for the Dark Energy Spectroscopic Instrument, Astron. J. 165, 50 (2023).
- [26] E. F. Schlafly, D. Kirkby, D. J. Schlegel, A. D. Myers, A. Raichoor, K. Dawson *et al.*, Survey operations for the Dark Energy Spectroscopic Instrument, Astron. J. **166**, 259 (2023).
- [27] DESI Collaboration, DESI DR2: Baryon acoustic oscillations from the Lyman alpha forest, arXiv:2503.14739.
- [28] U. Andrade *et al.*, Validation of the DESI DR2 baryon acoustic oscillations measurements from Galaxies and Quasars, arXiv:2503.14742.
- [29] A. G. Adame, J. Aguilar, S. Ahlen, S. Alam, D. M. Alexander *et al.* (DESI Collaboration), DESI 2024 III: Baryon acoustic oscillations from Galaxies and Quasars, J. Cosmol. Astropart. Phys. 04 (2025) 012.
- [30] A. G. Adame, J. Aguilar, S. Ahlen, S. Alam, D. M. Alexander *et al.* (DESI Collaboration), DESI 2024 IV: Baryon acoustic oscillations from the Lyman alpha forest, J. Cosmol. Astropart. Phys. 01 (2025) 124.
- [31] A. G. Adame, J. Aguilar, S. Ahlen, S. Alam, D. M. Alexander *et al.* (DESI Collaboration), DESI 2024 VI: Cosmological constraints from the measurements of baryon acoustic oscillations, J. Cosmol. Astropart. Phys. 02 (2025) 021.
- [32] N. Aghanim *et al.* (Planck Collaboration), Planck 2018 results. V. CMB power spectra and likelihoods, Astron. Astrophys. **641**, A5 (2020).
- [33] E. Rosenberg, S. Gratton, and G. Efstathiou, CMB power spectra and cosmological parameters from Planck PR4 with CamSpec, Mon. Not. R. Astron. Soc. **517**, 4620 (2022).
- [34] Y. Akrami, K. J. Andersen, M. Ashdown, C. Baccigalupi, M. Ballardini *et al.* (Planck Collaboration), Planck intermediate results. LVII. Joint Planck LFI and HFI data processing, Astron. Astrophys. **643**, A42 (2020).
- [35] E. McDonough, J. Colin Hill, M. M. Ivanov, A. La Posta, and M. W. Toomey, Observational constraints on early dark energy, Int. J. Mod. Phys. D **33**, 2430003 (2024).
- [36] G. Efstathiou, E. Rosenberg, and V. Poulin, Improved Planck constraints on axionlike early dark energy as a

- resolution of the Hubble tension, Phys. Rev. Lett. 132, 221002 (2024).
- [37] D. Rubin, G. Aldering, M. Betoule, A. Fruchter, X. Huang, A. G. Kim *et al.*, Union through UNITY: Cosmology with 2,000 SNe using a unified Bayesian framework, arXiv: 2311.12098.
- [38] H. Dembinski, P. Ongmongkolkul, and E. Al, scikit-hep/ IMINUIT, 2020, 10.5281/zenodo.4310361.
- [39] D. Foreman-Mackey, D. W. Hogg, D. Lang, and J. Goodman, EMCEE: The MCMC Hammer, Publ. Astron. Soc. Pac. 125, 306 (2013).
- [40] A. Lewis, GetDist: A Python package for analysing Monte Carlo samples, J. Cosmol. Astropart. Phys. 08 (2025) 025.
- [41] T. Karwal and M. Kamionkowski, Dark energy at early times, the Hubble parameter, and the string axiverse, Phys. Rev. D **94**, 103523 (2016).
- [42] V. Poulin, T. L. Smith, T. Karwal, and M. Kamionkowski, Early dark energy can resolve the Hubble tension, Phys. Rev. Lett. 122, 221301 (2019).
- [43] T. L. Smith, V. Poulin, and M. A. Amin, Oscillating scalar fields and the Hubble tension: A resolution with novel signatures, Phys. Rev. D 101, 063523 (2020).
- [44] L. Knox and M. Millea, Hubble constant Hunter's guide, Phys. Rev. D 101, 043533 (2020).
- [45] E. Abdalla, G. F. Abellán, A. Aboubrahim, A. Agnello, Ö. Akarsu, Y. Akrami *et al.*, Cosmology intertwined: A review of the particle physics astrophysics, and cosmology associated with the cosmological tensions and anomalies, J. High Energy Astrophys. **34**, 49 (2022).
- [46] V. Poulin, T. L. Smith, and T. Karwal, The ups and downs of early dark energy solutions to the Hubble tension: A review of models, hints and constraints circa 2023, Phys. Dark Universe **42**, 101348 (2023).
- [47] J.-Q. Jiang, Status of early dark energy after DESI: the role of  $\Omega_m$  and  $r_sH_0$ , Phys. Dark Universe **48**, 101902 (2025).
- [48] H. Kodama and M. Sasaki, Cosmological perturbation theory, Prog. Theor. Phys. Suppl. **78**, 1 (1984).
- [49] R. R. Caldwell, R. Dave, and P. J. Steinhardt, Quintessential cosmology novel models of cosmological structure formation, Astrophys. Space Sci. **261**, 303 (1998).
- [50] D. Blas, J. Lesgourgues, and T. Tram, The Cosmic Linear Anisotropy Solving System (CLASS). Part II: Approximation schemes, J. Cosmol. Astropart. Phys. 07 (2011) 034.
- [51] V. Poulin, T. L. Smith, D. Grin, T. Karwal, and M. Kamionkowski, Cosmological implications of ultralight axionlike fields, Phys. Rev. D 98, 083525 (2018).
- [52] J. Lesgourgues, The Cosmic Linear Anisotropy Solving System (CLASS) I: Overview, arXiv:1104.2932.
- [53] W. Hu and M. White, Acoustic signatures in the cosmic microwave background, Astrophys. J. 471, 30 (1996).
- [54] J. Silk, Cosmic black-body radiation and galaxy formation, Astrophys. J. **151**, 459 (1968).
- [55] M.-X. Lin, G. Benevento, W. Hu, and M. Raveri, Acoustic dark energy: Potential conversion of the Hubble tension, Phys. Rev. D 100, 063542 (2019).
- [56] J. C. Hill, E. McDonough, M. W. Toomey, and S. Alexander, Early dark energy does not restore cosmological concordance, Phys. Rev. D 102, 043507 (2020).

- [57] S. Vagnozzi, Consistency tests of ΛCDM from the early integrated Sachs-Wolfe effect: Implications for early-time new physics and the Hubble tension, Phys. Rev. D **104**, 063524 (2021).
- [58] A. G. Riess *et al.*, A comprehensive measurement of the local value of the Hubble constant with 1 km s<sup>-1</sup> Mpc<sup>-1</sup> uncertainty from the Hubble Space Telescope and the SH0ES team, Astrophys. J. Lett. **934**, L7 (2022).
- [59] W. L. Freedman, B. F. Madore, I. S. Jang, T. J. Hoyt, A. J. Lee, and K. A. Owens, Status report on the Chicago-Carnegie Hubble Program (CCHP): Three independent astrophysical determinations of the Hubble constant using the James Webb Space Telescope, Astrophys. J. 985, 203 (2025).
- [60] A. G. Riess, D. Scolnic, G. S. Anand, L. Breuval, S. Casertano, L. M. Macri *et al.*, JWST validates HST distance measurements: Selection of supernova subsample explains differences in JWST estimates of local H<sub>0</sub>, Astrophys. J. 977, 120 (2024).
- [61] T. J. Hoyt, I. S. Jang, W. L. Freedman, B. F. Madore, K. A. Owens, and A. J. Lee, The Chicago carnegie Hubble program: Improving the calibration of SNe Ia with JWST measurements of the tip of the red giant branch, arXiv: 2503.11769.
- [62] T. M. C. Abbott *et al.* (DES Collaboration), The Dark Energy Survey: Cosmology results with 1500 new highredshift Type Ia supernovae using the full 5-year dataset, Astrophys. J. Lett. 973, L14 (2024).
- [63] D. Scolnic *et al.*, The Pantheon + snalysis: The full data set and light-curve release, Astrophys. J. 938, 113 (2022).
- [64] M. Rigault, M. Smith, A. Goobar, K. Maguire, G. Dimitriadis, J. Johansson *et al.*, ZTF SN Ia DR2: Overview, Astron. Astrophys. 694, A1 (2025).
- [65] P. A. Abell, J. Allison, S. F. Anderson, J. R. Andrew, J. R. P. Angel *et al.* (LSST Science Collaboration), LSST science book, Version 2.0, arXiv:0912.0201.
- [66] P. Ade, J. Aguirre, Z. Ahmed, S. Aiola, A. Ali, D. Alonso *et al.*, The Simons Observatory: Science goals and forecasts, J. Cosmol. Astropart. Phys. 02 (2019) 056.
- [67] M. Abitbol, I. Abril-Cabezas, S. Adachi, P. Ade, A. E. Adler, P. Agrawal *et al.*, The Simons Observatory: Science goals and forecasts for the enhanced large aperture telescope, arXiv:2503.00636.
- [68] T. L. Smith, V. Poulin, and M. A. Amin, Oscillating scalar fields and the Hubble tension: A resolution with novel signatures, Phys. Rev. D 101, 063523 (2020).
- [69] M. M. Ivanov, E. McDonough, J. C. Hill, M. Simonović, M. W. Toomey, S. Alexander, and M. Zaldarriaga, Constraining early dark energy with large-scale structure, Phys. Rev. D 102, 103502 (2020).
- [70] M. Tristram, A. J. Banday, M. Douspis, X. Garrido, K. M. Górski, S. Henrot-Versillé *et al.*, Cosmological parameters derived from the final Planck data release (PR4), Astron. Astrophys. 682, A37 (2024).
- [71] H. Miyatake, S. Sugiyama, M. Takada, T. Nishimichi, X. Li, M. Shirasaki *et al.*, Hyper Suprime-Cam year 3 results: Cosmology from galaxy clustering and weak lensing with HSC and SDSS using the emulator based halo model, Phys. Rev. D 108, 123517 (2023).

- [72] C. Heymans, T. Tröster, M. Asgari, C. Blake, H. Hildebrandt, B. Joachimi *et al.*, KiDS-1000 cosmology: Multi-probe weak gravitational lensing and spectroscopic galaxy clustering constraints, Astron. Astrophys. **646**, A140 (2021).
- [73] T. M. C. Abbott, M. Aguena, A. Alarcon, S. Allam, O. Alves, A. Amon *et al.*, Dark energy survey year 3 results: Cosmological constraints from galaxy clustering and weak lensing, Phys. Rev. D 105, 023520 (2022).
- [74] J. McCullough, A. Amon, E. Legnani, D. Gruen, A. Roodman, O. Friedrich *et al.*, Dark energy survey year 3: Blue shear, arXiv:2410.22272.
- [75] A. H. Wright, B. Stölzner, M. Asgari, M. Bilicki, B. Giblin, C. Heymans *et al.*, KiDS-Legacy: Cosmological constraints from cosmic shear with the complete Kilo-Degree Survey, arXiv:2503.19441.
- [76] D. Alonso, G. Fabbian, K. Storey-Fisher, A.-C. Eilers, C. García-García, D. W. Hogg, and H.-W. Rix, Constraining cosmology with the Gaia-unWISE quasar catalog and CMB lensing: Structure growth, J. Cosmol. Astropart. Phys. 11 (2023) 043.
- [77] G. S. Farren, A. Krolewski, N. MacCrann, S. Ferraro, I. Abril-Cabezas, R. An *et al.*, The Atacama Cosmology Telescope: Cosmology from cross-correlations of unWISE galaxies and ACT DR6 CMB lensing, Astrophys. J. **966**, 157 (2024).
- [78] N. Sailer, J. Kim, S. Ferraro, M. S. Madhavacheril, M. White, I. Abril-Cabezas *et al.*, Cosmological constraints from the cross-correlation of DESI luminous red galaxies with CMB lensing from Planck PR4 and ACT DR6, J. Cosmol. Astropart. Phys. 06 (2025) 008.
- [79] R. de Belsunce, A. Krolewski, S. Chiarenza, E. Chaussidon, S. Ferraro, B. Hadzhiyska *et al.*, Cosmology from Planck CMB lensing and DESI DR1 quasar tomography, arXiv: 2506.22416.
- [80] S. Chen et al., Analysis of DESI × DES using the Lagrangian effective theory of LSS, Phys. Rev. D 110, 103518 (2024).
- [81] A. G. Adame, J. Aguilar, S. Ahlen, S. Alam, D. M. Alexander *et al.* (DESI Collaboration), DESI 2024 V: Full-shape galaxy clustering from galaxies and quasars, arXiv:2411.12021.
- [82] M. Maus, M. White, N. Sailer, A. Baleato Lizancos, S. Ferraro, S. Chen *et al.*, A joint analysis of 3D clustering and galaxy x CMB-lensing cross-correlations with DESI DR1 galaxies, arXiv:2505.20656.
- [83] G. Aricò, R. E. Angulo, M. Zennaro, S. Contreras, A. Chen, and C. Hernández-Monteagudo, DES Y3 cosmic shear down to small scales: Constraints on cosmology and baryons, Astron. Astrophys. 678, A109 (2023).
- [84] I. G. McCarthy, A. Amon, J. Schaye, E. Schaan, R. E. Angulo, J. Salcido et al., FLAMINGO: Combining kinetic SZ effect and galaxy-galaxy lensing measurements to gauge the impact of feedback on large-scale structure, arXiv: 2410.19905.

- [85] L. Bigwood, A. Amon, A. Schneider, J. Salcido, I. G. McCarthy, C. Preston et al., Weak lensing combined with the kinetic Sunyaev-Zel'dovich effect: a study of baryonic feedback, Mon. Not. R. Astron. Soc. 534, 655 (2024).
- [86] T. Ferreira, D. Alonso, C. Garcia-Garcia, and N. E. Chisari, X-ray-cosmic-shear cross-correlations: First detection and constraints on baryonic effects, Phys. Rev. Lett. 133, 051001 (2024).
- [87] B. Hadzhiyska, S. Ferraro, and R. Zhou, Tracing cosmic gas in filaments and halos: Low-redshift insights from the kinematic Sunyaev-Zel'dovich effect, Phys. Rev. D 111, 023534 (2025).
- [88] G. Piccirilli, M. Zennaro, C. García-García, and D. Alonso, Robust cosmic shear with small-scale nulling, arXiv:2502 .17339.
- [89] D. Anbajagane, C. Chang, Z. Zhang, C. Y. Tan, M. Adamow, L. F. Secco *et al.*, The DECADE cosmic shear project I: A new weak lensing shape catalog of 107 million galaxies, arXiv:2502.17674.
- [90] K. Bechtol, I. Sevilla-Noarbe, A. Drlica-Wagner, B. Yanny, R. A. Gruendl, E. Sheldon *et al.*, Dark energy survey year 6 results: Photometric data set for cosmology, arXiv:2501 .05739.
- [91] L. Amendola, S. Appleby, A. Avgoustidis, D. Bacon, T. Baker, M. Baldi *et al.*, Cosmology and fundamental physics with the Euclid satellite, Living Rev. Relativity 21, 2 (2018).
- [92] N. G. Karaçaylı *et al.*, Optimal 1D Ly $\alpha$  forest power spectrum estimation—III. DESI early data, Mon. Not. R. Astron. Soc. **528**, 3941 (2024).
- [93] R. de Belsunce, O. H. E. Philcox, V. Iršič, P. McDonald, J. Guy, and N. Palanque-Delabrouille, The 3D Lyman- $\alpha$  forest power spectrum from eBOSS DR16, Mon. Not. R. Astron. Soc. **533**, 3756 (2024).
- [94] R. Bacon, V. Maineiri, S. Randich, A. Cimatti, J.-P. Kneib, J. Brinchmann *et al.*, WST—Widefield Spectroscopic Telescope: Motivation, science drivers and top-level requirements for a new dedicated facility, Proc. SPIE Int. Soc. Opt. Eng. **13094**, 1309410 (2024).
- [95] R. Besuner, A. Dey, A. Drlica-Wagner, H. Ebina, G. Fernandez Moroni, S. Ferraro *et al.*, The spectroscopic stage-5 experiment, arXiv:2503.07923.
- [96] T. Louis, A. La Posta, Z. Atkins, H.T. Jense, I. Abril-Cabezas, G. E. Addison *et al.*, The Atacama Cosmology Telescope: DR6 power spectra, likelihoods and ΛCDM parameters, arXiv:2503.14452.
- [97] E. Calabrese, J. C. Hill, H. T. Jense, A. La Posta, I. Abril-Cabezas, G. E. Addison *et al.*, The Atacama Cosmology Telescope: DR6 constraints on extended cosmological models, arXiv:2503.14454.
- [98] https://www.desi.lbl.gov/collaborating-institutions
- [99] E. Chaussidon, Early time solution as an alternative to the late time evolving dark energy with DESI DR2 BAO, https://zenodo.org/records/15185439.